Porous methacrylate tissue engineering scaffolds: using carbon dioxide to control porosity and interconnectivity

JOHN J. A. BARRY, MARTA M. C. G. SILVA
School of Chemistry, University of Nottingham, University Park, Nottingham, NG7 2RD, UK

SARAH H. CARTMELL, ROBERT E. GULDBERG
Orthopaedic Bioengineering Laboratory, Woodruff School of Mechanical Engineering, Georgia Institute of Technology, 315 Ferst Drive, NW IBB Building, Room 2311, Atlanta, GA, 30332-0405, USA

COLIN A. SCOTCHFORD
School of Biomedical Sciences, University of Nottingham Medical School, Queen's Medical Centre, Nottingham, NG7 2UH, UK; Bioengineering Section, School of Mechanical, Materials, Manufacturing Engineering and Management, University of Nottingham, Nottingham, NG7 2RD, UK

STEVEN M. HOWDLE*
School of Chemistry, University of Nottingham, University Park, Nottingham, NG7 2RD, UK
E-mail: steve.howdle@nottingham.ac.uk

Published online: 15 May 2006

Porous scaffold structures are used in tissue engineering to provide structural guidance for regenerating tissues. The use of carbon dioxide (CO_2) to create such scaffolds has received some attention in the past but many researchers believe that although CO_2 processing of polymers can lead to porous scaffolds there is limited interconnectivity between the pores. In this study, highly porous (greater than 85%) and well interconnected scaffolds were obtained in which the size, distribution and number of pores could be controlled. This control was achieved by altering the rate of venting from polymer discs saturated with CO_2 under modest temperature and pressure. The polymer used is a blend of poly (ethyl methacrylate) and tetrahydrofurfuryl methacrylate (PEMA/THFMA). This polymer system has shown promise for potential applications in cartilage repair.

Introduction

Scaffolds are three-dimensional structures that are used in tissue engineering studies to aid growth and differentiation of cells. The manufacture of porous polymer scaffolds has been achieved using a number of novel technologies (for review see [1]). However the use of organic solvents is commonplace in these methods and often results in solvent residues remaining post-processing. Such residues are then capable of leaching out from scaffolds and damaging cells and nearby tissues. Because scaffolds should be non-mutagenic, non-carcinogenic, non-toxic and non-teratogenic there is much interest in solvent-free methods of processing [2]. Solvent free methods include; mechanical stretching, fibre extrusion and bonding, template synthesis, phase separation and the use of gases as porogens [3].

An example of a gas that has been previously used as a porogen is carbon dioxide (CO_2). Above a critical temperature ($T_c = 31.1°C$) and pressure ($P_c = 73.8$ bar) CO_2 demonstrates both gas and liquid properties and it is the unique properties of supercritical carbon dioxide ($scCO_2$) that allow the gas to be used as a processing medium for the production of either fine particles or to function as a porogen in the production of porous foams [4–8]. The polymers, poly (methyl methacrylate), polystyrene, polycarbonate poly (ethylene terepthalate) and more

*Author to whom all correspondence should be addressed.
0022-2461
DOI: 10.1007/s10853-006-7023-8

recently the biomedical polymers poly(D,L-lactide) (PLA) and poly(D,L-lactide-co-glycolide) (PLGA) have all been foamed using $scCO_2$ [1, 7–12].

Many researchers working with CO_2 believe that the processing results in the formation of highly porous scaffolds but with limited connectivity between pores [2, 3, 9, 13]. More recently it has been demonstrated that pore architecture can be affected by altering the parameters that control pore generation. The controlling variables are temperature, pressure and rate of venting [10, 14–16]. The effect of vent rate on a non-degradable polymer system consisting of poly(ethyl methacrylate)/tetrahydrofurfuryl methacrylate (PEMA/THFMA) is the subject of this study. The PEMA/THFMA polymer system is a room temperature polymerising blend consisting of a polymer powder (PEMA) to which liquid monomer (THFMA) is added (Fig. 1). Unreacted residual benzoyl peroxide (BPO) present in the PEMA initiates the reaction. However for this to occur a co-initiator dimethyl-*para*-toluidene; (DMPT) must be present to initiate the decomposition of BPO to peroxide radicals.

Non-porous PEMA/THFMA has previously been investigated as a cartilage repair material both *in vivo* and *in vitro* [17–22]. *In vitro* studies have demonstrated that the material can support bovine chondrocyte growth and differentiation. *In vivo* studies have demonstrated that rabbit osteochondral defects were filled with dense cartilagenous tissue when this material was placed in the defect. Initial studies of the foamed PEMA/THFMA have further demonstrated that chondrocyte growth and differentiation was increased with respect to the unfoamed material [23]. Studies on the surface chemistry of PEMA/THFMA demonstrate that the material appears to present adsorbed fibronectin in a more favourable conformation to support cell adhesion when compared to other polymers [24].

The purpose of this study is to investigate how changes in the processing by $scCO_2$ can affect porosity, pore size, pore interconnectivity and mechanical properties of porous scaffolds. The ultimate aim is to construct PEMA/THFMA polymer scaffolds that have optimum porosity, pore size and pore interconnectivity for tissue engineering purposes.

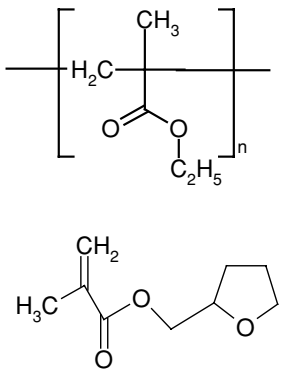

Figure 1 Structures of poly(ethyl methacrylate) (*top*) and the monomer tetrahydrofurfuryl methacrylate (*bottom*).

Experimental

Preparation of the PEMA/THFMA discs

PEMA/THFMA polymer discs were made by mixing PEMA powder (5 g, Bonar Polymers Ltd, Newton Aycliffe, UK) and THFMA, monomer liquid (3 ml, Rohm Chemie, Darmstadt, Germany). N,N-dimethyl-p-toluidine (DMPT) was added, (2.5% v/v) to effect polymerisation. This mixture was placed in a custom fabricated PTFE mould and was left overnight to polymerise, producing discs 10 mm in diameter and 10 mm thickness.

Foaming was achieved as follows. Discs were placed into a 10 ml Thar extraction vessel and saturated with CO_2 at 1470 psi (100 bar) at 40°C for a period of 8 h. Following this exposure, the $scCO_2$ was vented over 30 s, 15 or 60 min. Control of the venting rate was maintained by a backpressure regulator (Jasco UK, Model BPR-1580-81).

The foamed discs were removed from the vessel and cut to produce discs 10 mm in diameter and 3 mm in thickness. Pore size, percentage porous material and interconnectivity of pores were determined using scanning electron microscopy (SEM), mercury intrusion porosimetry, helium pycnometry and micro-computed tomography (micro-CT) respectively.

Sem

The cellular morphologies of the foamed samples were investigated using a Philips XL-30 SEM. The samples were freeze fractured in liquid nitrogen and sputter coated with gold at an Argon pressure of 13 Pa for 3 min at a current rate of 14 mA. The diameter (across the mouth of the pores) was determined using standard XL-30 software. Pores were counted randomly beginning at the centre and travelling set distances from this point. A minimum sample size of 100 was counted. Histograms of the frequency of each diameter were constructed to determine the pore size distribution and the mean pore diameter. The pore nucleation densities were determined using Equation 1 [14].

$$(N) = ((\rho_u/\rho_f) - 1)/\Pi D^3/6 \quad (1)$$

Where N is the pore density, ρ_u and ρ_f are the densities of the unfoamed and foamed materials and D^3 is the mean pore diameter.

Mercury porosimetry

The pore size distribution and the average pore size were calculated using mercury porosimetry (Micromeritics Accupore IV) at pressures ranging from 0–25 psi. Mercury porosimetry was also employed to calculate the permeability of the material using the manufacturers' software.

Helium pycnometry

Helium pycnometry employs Archimedes' principle of fluid displacement to calculate density. A Micromeritics AccuPyc 1330 Pycnometer was used to calculate the

density of the foams ($\rho_{\text{pycnometry}}$) and the absolute density of the unfoamed PEMA/THFMA (ρ_{unfoamed}).

The total (Equation 2) and the closed (Equation 3) porosity of the material, was calculated using published formulae [13, 25]. These formulae relate the porosity (P) to the densities (ρ) of the foamed material.

Gross measurements and weight were used to calculate the geometric density $\rho_{\text{geometric}}$. $\rho_{\text{geometric}} = m/v$, where m is the mass and v is the volume of the foamed PEMA/THFMA disc. The volume of the discs was calculated using the equation $v = \pi r^2 h$ where r is the radius of the disc and h is the height. The mean disc height and diameter were measured using standard engineering calipers (Mitutoyo UK Ltd.).

$$\varepsilon_{\text{total}} = (1 - (\rho_{\text{geometric}}/\rho_{\text{unfoamed}})) \times 100 \quad (2)$$

$$\varepsilon_{\text{total}} = (1 - (\rho_{\text{pycnometry}}/\rho_{\text{unfoamed}})) \times 100 \quad (3)$$

Microarchitectural analysis

Briefly, a micro-CT system μCT 40 (Scanco Medical, Bassersdorf, Switzerland) was used to non-destructively image and quantify the 3D microstructural morphology and anisotropy of each sample [26]. Samples were scanned at 20 μm voxel resolution with an integration time of 120 ms to produce 3D reconstructed images. From these images, structural indices were calculated using 3D algorithms that do not rely on model-assumptions of the local microstructure [27, 28]. In addition to overall porosity, the average pore size in each scaffold was calculated as the mean diameter of maximally-sized spheres fitting within the pore spaces.

Compressive strength and modulus

Mechanical data were obtained through compression testing using a Lloyd tensile testing machine (Model M30 K). Scaffolds were analysed as prepared and variations in diameter, depth and weight noted. A minimum of six scaffolds was tested at a cross head speed of 1 mm/s and extension of 20 mm. A full scale load of 3 KN was used for the scaffolds. Load extension graphs were obtained during testing and converted to stress strain curves applying Equations 4 and 5.

$$\text{Stress} = \sigma = F/A \quad (4)$$

$$\text{Strain} = \varepsilon = \Delta L/L \quad (5)$$

Where F is the applied force, A is the cross sectional area, ΔL is the change in length and L is the original length.

Results and discussion

The main aim of this study was to create porous PEMA/THFMA foams that could be employed as tissue engineering scaffolds. In order for these foams to be

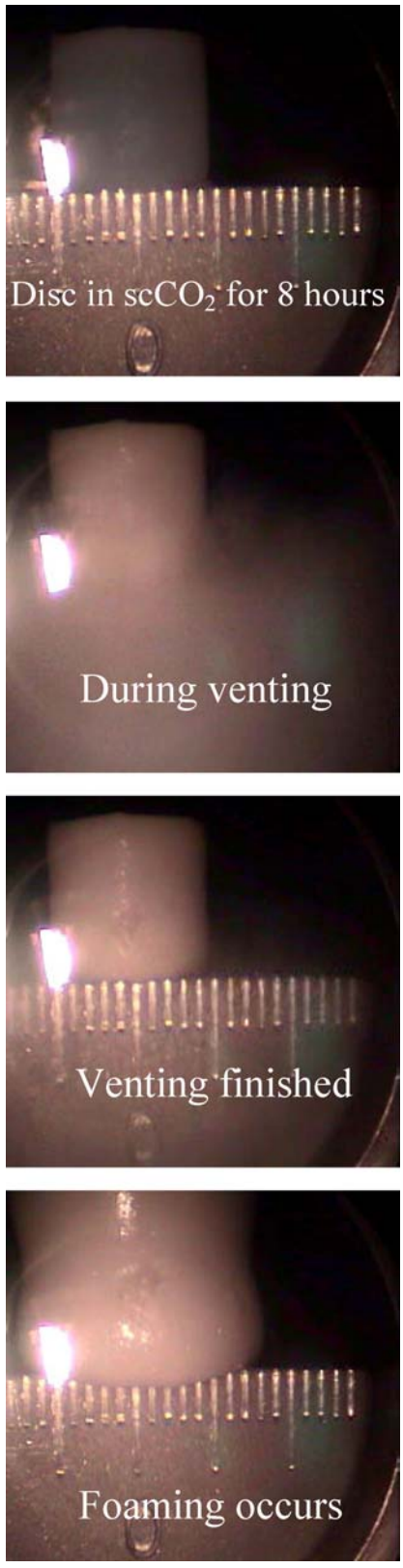

Figure 2 The *in-situ* foaming of PEMA/THFMA. The photographs are taken through a high pressure vessel sapphire window. The polymer remains structurally unchanged until nearly all the carbon dioxide gas has been vented and then the polymer foams. In these images the internal diameter of the vessel has been restricted by the incorporation of a graduated scale (mm markings).

utilized as scaffolds they would have to satisfy a number of structural criteria that govern the suitability of a scaffold as a tissue engineering device. These include adequate porosity, pore size, pore interconnectivity, mechanical properties, and a surface chemistry that permits cell attachment, proliferation and differentiation.

$ScCO_2$ foaming of polymers takes place when the polymer becomes saturated with CO_2 gas at a given temperature. This causes a depression in the glass transition (T_g) and plasticization of the polymer. The solubility of the gas in the polymer is decreased as CO_2 pressure is released whilst maintaining constant temperature (isothermal). Two physical events occur to give rise to the polymeric foams. The first is the sudden reduction in pressure leading to the generation of nuclei (or bubbles). These nuclei grow to form the pores in the foam. The porous structures then become fixed by the second event, the rise in T_g as the plasticization effect is lost. When the T_g rises above the processing temperature, the pores can grow no further and are "locked in" [9, 14, 29, 30].

When the polymer is plasticized, nucleation is usually accompanied by and competes with diffusion of gas into pores. This diffusion of gas into the pores results in pore growth. If the venting rate is fast, then nucleation is rapid and the number of nucleation sites large. Pores will develop so fast that the diffusion effects will be negligible and the resultant structure will have a homogeneous or uniform pore size distribution. On the other hand, if nucleation is very slow, the pores nucleated first will be significantly larger than others due to greater diffusion of gas to those pores from the surrounding matrix, and the resultant structure will have wide pore size dispersity [31].

In this study the foaming of the PEMA/THFMA discs changed their appearance from glassy and opaque to larger discs that were white in appearance (Fig. 2). The sequence of photographs demonstrates the foaming of PEMA/THFMA is different to the foaming of biodegradable polyesters described elsewhere [9, 32]. The foaming of PLA and PLGA takes place after the polymer liquefies in CO_2 to form a polymer/gas solution [32]. By contrast, the PEMA/THFMA, remains structurally intact until almost all the gas has been released from the vessel and then the polymer foams.

A relationship between exposure time and the degree of foaming was observed. This degree of foaming has been quantified using a term previously described by Nikitin [33]. The term is identified in this study as the foaming factor (FF) and was calculated using Equation 6, where V_f is the volume of the foamed discs and V_0 is the volume of the unfoamed disc.

$$\mathrm{FF} = \frac{V_f - V_0}{V_0} \tag{6}$$

The relationship between FF and exposure time (Fig. 3) demonstrates that FF rises quite steeply and then begins to level off at about the 8 h mark. This upper limit was not due to the material, but was a restriction imposed by the vessel. Using a high pressure vessel with a larger volume (60 ml), it was demonstrated that the discs were capable of further expansion (Fig. 3).

As there is already a wealth of research into foaming in relation to changes in temperature and pressure, this study has focussed solely on the manipulation of CO_2 release as the method of controlling the scaffold characteristics. Increasing the pressure increases the number of nucleation sites [14] whereas controlling the vent rate allows the nucleation sites to grow into pores while also allowing the pores to coalesce, thereby altering pore size and interconnectivity. Representative electron micrographs of the foams made by the different venting rates are shown in Fig. 4a–c. Clear differences in the average pore size, pore density (the number of pores per cm^3) and pore size distribution can be determined reproducibly for each set of processing conditions (Table I). In the 30 s vent, nucleation occurs rapidly resulting in small pores ranging from ca. 10–350 μm with a narrow distribution (>75% of the pores were within 50–150 μm). In the slower 15 and 60 min vents the pores are allowed to grow and to merge into each other, creating large pores with very broad distributions; in the range 20–1700 μm. For the 15 min vents most of the pores (i.e. >75%) lie in the range 150–650 μm. By contrast, when vented over 60 min most pores (>75%)

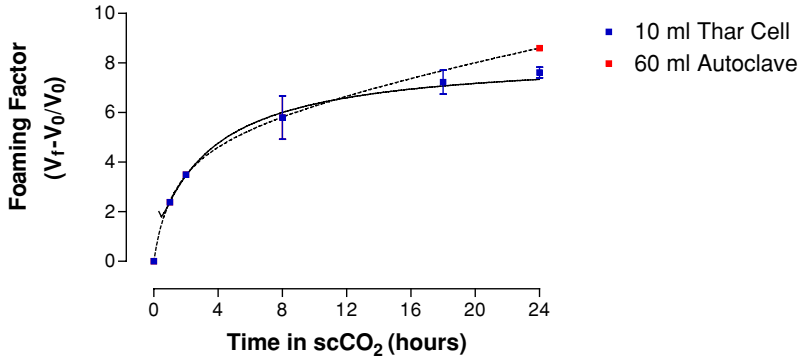

Figure 3 The relationship between foaming factor (FF) and the length of exposure to $scCO_2$. The solid line demonstrates the FF in the 10 ml high pressure vessel. While the dotted line shows the FF in a vessel with a much larger volume in which the swelling was unrestricted.

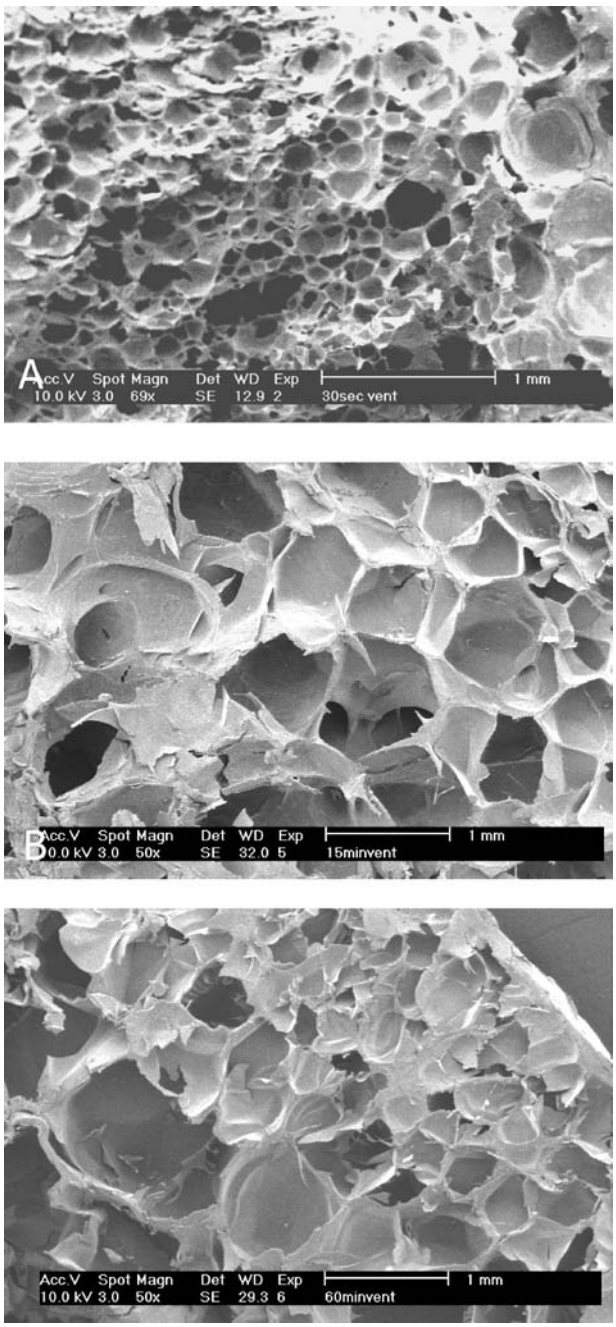

Figure 4 Electron micrographs of PEMA/THFMA that have been exposed to $scCO_2$ for 8 h @ 100 bar/40°C. The samples have been vented at different rates leading to controlled differences in pore sizes (a) fast vent (30 s) showing small pores of the order of 100 μm. (b) Intermediate vent (15 min) showing pores in the region of 350 μm. (c) Slow vent (60 min) showing a mixture of very large and small pores.

lie within 200–900 μm. All samples were highly porous with bifurcations into adjacent pores visible. The 60 min vented samples proved most difficult to analyse due to damage to the weak cellular structure in the preparation for SEM.

Pore diameters calculated by micro-CT analysis (Fig. 5, Table I) correlated well with those obtained by SEM but, values obtained by porosimetry were significantly smaller (Table I). There are a number of reasons that may explain this observation; (1) it is quite common to use assumed contact angles for mercury porosimetry and this may lead to errors, (2) to make the measurements the porosimeter compresses the mercury into the porous material this can lead to compression or even damage of the overall structure and (3) in order to access a certain pore, the mercury may need to be forced through a pore opening smaller than the pore diameter. In this case the diameter calculated will be attributed to the pores aperture rather than the pore smaller diameters [34]. Despite the reported differences in pore diameter, both porosimetry and SEM demonstrate that there is clearly an increase in pore size and a significant broadening of the pore distribution as the vent time increases.

Different tissues appear to have different requirements for optimal pore sizes. For fibroblasts and hepatocytes optimum pore sizes of between 20 and 125 μm have been suggested [35] whereas for skin regeneration a range of 100–250 μm has been recommended. For bone regeneration pore sizes in the range 200–400 μm are believed to provide the most favourable curvature for optimum compression and tension on cell mechanoreceptors [36]. Thus the ability to tailor a scaffold to a particular pore diameter as shown by changing the vent time will increase the potential range of potential uses for a particular scaffold. Another important factor in determining the suitability of a scaffold is the pore aperture. Ultimately this will impact upon cell and tissue ingress into the scaffold thus mercury porosimetry may provide valuable information here.

The porosity of a scaffold is the fraction of the bulk volume of the porous sample that is occupied by void space. This void space can be connected to other pores or can be closed [37]. Scaffolds require a porosity of at least 70% and this porosity should be highly interconnected to aid in the delivery of cell nutrients and removal of metabolic waste as well as aid in tissue in-growth. The porous PEMA/THFMA scaffolds that have been generated in this study were found to have total porosities (ε_{total}) greater than 80% and this increased with longer venting times (range 81–90% as determined by densities (Table II). The effective or open porosity (ε_{open}) also varied with venting time ranging from 58% to greater than 70% as the venting time increased (Table II). The total porosity and open porosity increased rapidly reaching a plateau at the 15 min vent, beyond which any increase in venting time did not significantly alter the open porosity. The increases in open porosity described here may be attributable to the foams becoming fixed or "locked in" at the point at which coalescence of the pores occurs.

A relationship was also observed between the open porosity and permeability (Fig. 6). Permeability is the ability of a fluid under pressure to flow through a porous material. Clearly, fluid flow through a scaffold will be important to its function and permeability has been investigated recently as a method of assessing pore inter- connectivity in bone [38–40] and polymeric scaffolds [41]. The relationship between open porosity and permeability observed in this study of PEMA/THFMA

TABLE I. Changes in the foaming characteristics as measured by foaming factor (FF), mean pore diameter and pore density (number of pores per cm^3), corresponding to changes in venting rate. Mean pore diameters as determined by electron microscopy (SEM), micro-computed tomography (μCT) and mercury intrusion porosimetry. SEM and μCT returned similar values whereas porosimetry calculated the pore sizes to be significantly smaller. Where relevant the results are presented as mean + std deviatio

	Processing conditions; 8 h @ 100 Bar/ 40°C		
	30 s vent	15 min vent	60 min vent
Foaming factor ($V_f - V_0/V_0$)	4.3 ± 0.7	6.5 ± 0.8	7.4 ± 0.6
Pore diameter (μm)			
SEM	97	350	450
μCT	140	400	650
Porosimetry	35	120	175
Pore density (pores/cm^3)	$95.7 \times 10^5 \pm 14.5 \times 10^5$	$2.21 \times 10^5 \pm 0.24 \times 10^5$	$1.42 \times 10^5 \pm 0.13 \times 10^5$

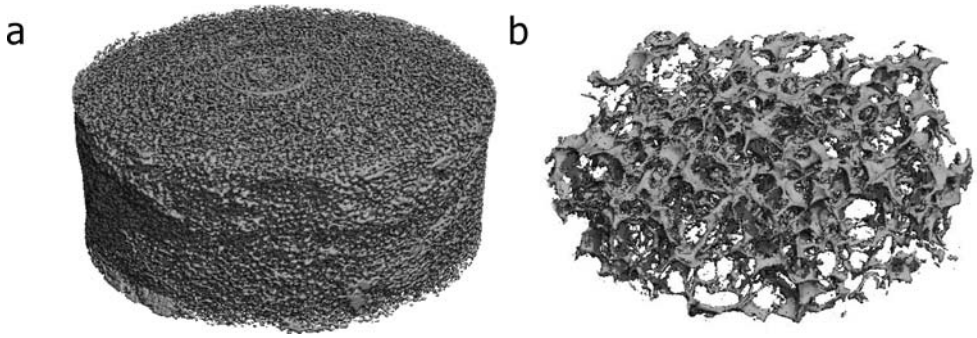

Figure 5 Micro-CT images of a) the 30 s and b) 60 min vented scaffolds. These images correspond with columns 2 and 4 in Table I. Changes in porosity, pore size and interconnectivity are clearly visible from the images.

scaffolds was found to be similar to those previously observed for bone [42]. Permeability values in the current study were in the range 7.3–21.5 $\times 10^{-9}$ m^2 and compare well with were those previously observed in calcaneal trabecular bone (0.4–11 $\times 10^{-9}$ m^2) and human proximal tibia (3–16 $\times 10^{-9}$ m^2) [38–40]. The lack of a linear relationship between open porosity and permeability in this study (Fig. 6) does suggest that there are other factors in addition to porosity to be considered such as pore size, connectivity of pores and the tortuous path taken by fluid (tortuosity) within the scaffold. Others have suggested that permeability is a specific property of macroporous materials and is independent of sample size and fluid used [41]. They have also suggested that since there is a threshold for cell ingrowth; i.e. no tissue grows in pores smaller than 5 μm, "further studies should take place to determine if a threshold for permeability exists" [41].

The mechanical properties corresponding to each of the vent times were also assessed. The compressive yield point is the point at which the stress and strain are no longer linear. It marks the onset of plastic deformation in the polymer. The compressive yields for the scaffolds were found to decrease at longer vent times i.e the scaffolds were became weaker (Table II).

Pore modelling has identified that a reciprocal relationship exists between mechanical strength and pore diameter and porosity [43]. In other polymeric scaffolds compressive strengths in excess of 5 MPa have been produced [44]. However the porosity of such material was relatively low at 28.5%. By contrast a technique that combines CO_2 foaming and salt leaching produced 95% porous PLGA scaffolds with compressive moduli of 289 ± 25 kPa [13]. The scaffolds produced in this study have markedly higher compressive moduli, at only slightly lower porosity levels (Table II).

TABLE II. The densities calculated using gravimetry and pycnometry and the porosities calculated using the densities. The density of unfoamed PEMA/THFMA 1.12 g/cm^3 measured by pycnometry. The compressive strengths obtained using uniaxial compression testing of the materials are presented in the last column. Results are presented as mean or mean + std dev

	Density (g/cm^3)		Porosity (%)			
	Geometric	Pycnometry	Total	Closed	Open	Comp. Strength (MPa)
30 s vent	0.1921	0.8335	81.7 ± 2.9	24.3 ± 13.5	57.3 ± 13.5	2.67 ± 0.38
15 min vent	0.1408	1.0592	87.4 ± 1.2	10.3 ± 10.5	79.0 ± 9.5	1.5 ± 0.6
60 min vent	0.1285	0.9173	88.5 ± 1.0	14.6 ± 9.8	73.5 ± 9.0	0.55 ± 0.27

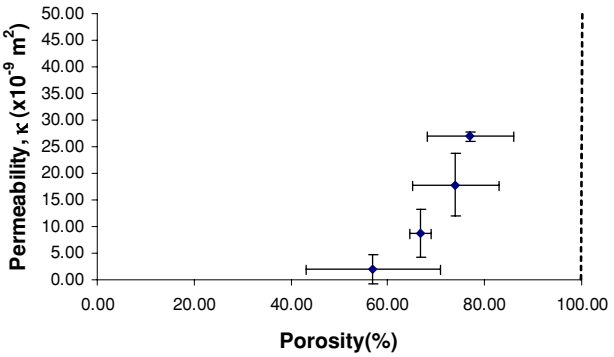

Figure 6 Relative permeability versus the open porosity for PEMA/THFMA scaffolds. As the porosity of the scaffold increases the permeability of the scaffold to fluid flow also increases.

Conclusion

This study described the preparation of scaffolds from a material that has previously shown potential to aid cartilage repair. A combination of techniques was applied to determine the key characteristics of the scaffolds produced. SEM and micro-CT images have been used to obtain the scaffold pore size and pore size distribution. Additionally micro-CT and gravimetric techniques can be used to measure the total porosities and the interconnectivity can then be assessed by pycnometry. Mercury intrusion porosimetry (MIP) has generally been regarded as an unsuitable method for scaffold characterisation and the porosity and pores size distribution did not correlate well with SEM and micro-CT. However MIP can be used effectively to measure pore apertures and the permeability of the scaffolds, thus allowing investigation of the relationship between permeability and pore connectivity.

This study has also demonstrated that $scCO_2$ processing of the PEMA/THFMA polymer offers a route to creating highly interconnected porous structures in which the size, distribution and number of pores can be controlled by manipulation of the rate of depressurisation. There is however an upper limit to these changes in pore architecture beyond which no further benefit can be seen. When this limit is exceeded the pore sizes and mechanical strengths make them unsuitable for use as scaffolds. Future studies will focus upon cell culture and applications to tissue engineering.

Acknowledgments

This work made use of ERC Shared Facilities supported by the National Science Foundation under Award Number EEC-9731643. We thank Professors K.M. Shakesheff, and AI Cooper, Dr. Dan Bratton, Mr. P. Fields and Mr. R. Wilson for their help and advice. We thank the BBSRC for financial support (JJAB). SMH is a Royal Society Wolfson Research Merit Award Holder.

References

1. G. CHEN, T. USHIDA and T. TATEISHI, *Macromol. Biosci.* **2** (2002) 67.
2. K. F. LEONG, C. M. CHEAH and C. K. CHUA, *Biomaterials* **24** (2003) 2363.
3. Q. HUANG, D. PAUL and B. SEIBIG, *Membrane Technol.* **140** (2001) 6.
4. R. A. QUIRK, R. M. FRANCE, K. M. SHAKESHEFF and S. M. HOWDLE, *Curr. Opin. Solid State Mater. Sci.* **8** (2004) 313.
5. M. WEBER, L. RUSSELL and P. DEBENEDETTI, *J. Supercritical Fluids* **23** (2002) 65.
6. M. A. MCHUGH and V. J. KRUKONIS, Supercritical Fluid Extraction: Principles and Practice (Butterworth-Heinemann, Boston, 1994), p 512.
7. A. I. COOPER, *Adv. Mater.* **13** (2001) 1.
8. H. M. WOODS, M. M. C. G. SILVA, C. NOUVEL, K. M. SHAKESHEFF and S. M. HOWDLE, *J. Mater. Chem.* **14** (2004) 1663.
9. D. J. MOONEY, D. F. BALDWIN, N. P. SUH, J. P. VACANTI and R. LANGER, *Biomaterials* **17** (1996) 1417.
10. S. M. HOWDLE, *et al. Chem. Commun.* **1** (2001) 109.
11. S. G. KAZARIAN, *Polym. Sci.* **42** (2000).
12. D. L. TOMASKO, *et al. Ind. Eng. Chem.* **42** (2004) 6431.
13. L. D. HARRIS, B.-S. KIM and D. J. MOONEY, *J. Biomed. Mater. Res.* **42** (1998) 396.
14. S. K. GOEL and E. J. BECKMAN, *Polym. Eng. Sci.* **34** (1994) 1137.
15. *Ibid.*, **34** (1994) 1148.
16. C. B. PARK, D. F. BALDWIN and N. P. SUH, *ibid.*, **35** (1995) 432.
17. S. DOWNES, R. S. ARCHER, M. V. KAYSER, M. P. PATEL and M. BRADEN, *J. Mater. Sci.: Mater. Med.* (1994) 88.
18. N. REISSIS, S. DOWNES, M. KAYSER, D. LEE and G. A. BENTLEY, *ibid.*, **5** (1994) 793.
19. *Ibid.*, **5** (1994) 402.
20. R. M. SAWTELL, S. DOWNES and M. V. KAYSER, *ibid.*, **6** (1995) 676.
21. R. M. SAWTELL, M. V. KAYSER and S. DOWNES, *Cells Mater.* **5** (1995) 63.
22. R. M. WYRE and S. DOWNES, *Biomaterials* **21** (2000) 335.
23. J. J. A. BARRY, H. S. GIDDA, C. A. SCOTCHFORD and S. M. HOWDLE, *ibid.* **25** (2004) 3559.
24. C. D. MCFARLAND, *et al.*, *J. Biomed. Mater. Res.* **44** (1999) 1.
25. A. TAMPIERI, G. CELOTTI, S. SPRIO, A. DELCOGLIANO and S. FRANZESE, *Biomaterials* **22** (2001) 1365.
26. Y. DAUSSE, *et al.*, *Osteoarthritis Cartilage* **11** (2003) 16.
27. T. HILDEBRAND and P. RUEGSEGGER, *J. Microsc.* **185** (1997) 67.
28. T. HILDEBRAND, A. LAIB, R. MULLER, J. DEQUEKER and P. RUEGSEGGER, *J. Bone and Mineral Res.* **14** (1999) 1167.
29. A. I. COOPER, *J. Mater. Chem.* **10** (2000) 207.
30. K. A. ARORA, A. J. LESSER and T. J. MCCARTHY, *Macromolecules* **31** (1998) 4614.
31. S. H. ALAVI, B. K. GOGOI, M. KHAN, B. J. BOWMAN and S. S. H. RIZVI, *Food Res. Int.* **32** (1999) 107.
32. M. C. G. S. SILVA, K. M. SHAKESHEFF and S. M. HOWDLE, Polymer scaffolds for cartilage engineering using supercritical fluids. in *UKSB Conf. Proc.* (Northern Ireland, 2003).
33. L. N. NIKITIN, *et al.*, *Macromol* **35** (2002) 934.
34. C. A. LEÓN Y LEÓN, *Adv. Colloid and Interface Sci.* **76-77** (1998) 341.
35. I. V. YANNAS, E. LEE, D. P. ORGILL, E. M. SKRABUT and G. F. MURPHY, *Proc. Natl. Acad. Sci.* **86** (1989) p. 933.
36. B. D. BOYAN, T. W. HUMBERT, D. D. DEAN and Z. SCHWARTZ, *Biomater.* **17** (1996) 137.
37. F. A. L. DULLIEN, "Porous Media: Fluid Transport and Pore Structure" (Academic Press, San Diego, 1992), p. 574.

38. P. W. HUI, P. C. LEUNG and A. SHER, *J. Biomech.* **29** (1996) 123.
39. M. J. GRIMM and J. L. WILLIAMS, *ibid.* **30** (1997) 743.
40. J. SOHIER, R. E. HAAN, K. DE GROOT and J. M. BEZEMER, *J. Control. Release* **87** (2003) 57.
41. S. LI, J. R. DE WIJN, J. LI, P. LAYROLLE and K. DE GROOT, *Tissue Eng.* **9** (2003) 535.
42. G. BAROUD, J. Z. WU, M. BOHNER, S. SPONAGEL and T. STEFFEN, *Med. Eng. Phys.* **25** (2003) 283.
43. L. J. GIBSON and M. F. ASHBY, "Cellular Solids: Structure and Properties" (Cambridge University Press, Cambridge, 1997).
44. A. S. P. LIN, T. H. BARROWS, S. H. CARTMELL and R. E. Guldberg, *Biomater.* **24** (2003) 481.

Received 20 December
and accepted 1 September 2005